Preparation, Structure and Spectroscopic Properties of NH4[Ln(S2CNH2)4]·H2O (Ln=La, Eu)

Christoph L. Teske,*[a] Ercules E. S. Teotonio,[a, b] Huayna Terraschke,[a] Sebastian Mangelsen,[a] and Wolfgang Bensch[a]

The title compounds were prepared under mild ambient conditions by a facile co-precipitation route. $NH_4[Eu(S_2CNH_2)_4]\cdot H_2O$ (**a**) and $NH_4[La(S_2CNH_2)_4]\cdot H_2O$ (**b**) crystallize isotypically in the monoclinic space group $P2_1/c$ with $a=$ 8.4461(3), $b=13.6367(3)$, $c=16.2945(5)$ Å, $\beta=103.759(2)°$ (for (**a**)), and $a=8.50484(9)$, $b=13.84476(16)$, $c=16.20816(17)$ Å, $\beta=103.7644(11)°$ for (**b**), respectively. The spectroscopic data reveal the presence of a **l**igand-to-**m**etal **c**harge **t**ransfer (LMCT) process of low energy in **a** and in the solid solutions $NH_4[La_{1-x}Eu_x(S_2CNH_2)_4]\cdot H_2O$ (x=0.016 and 0.05). Despite of the

consequent efficient luminescent quenching, it was possible to recorded excitation and emission spectra at room temperature. These spectra are characterized by narrow bands due to intraconfigurational-4f transitions of the Eu^{3+} ion. However, broad bands associated to the LMCT state were also observed, mainly for the solid solutions $NH_4[La_{1-x}Eu_x(S_2CNH_2)_4]\cdot H_2O$ (x= 0.016 and 0.05). Consequently, an intramolecular energy transfer mechanism is proposed, taking into account the role of the LMCT on the spectroscopic properties of dithiocarbamate complexes.

Introduction

Lanthanide dithiocarbamate compounds have gained special attention due to their potential applications in different areas, ranging from catalysis[1,2] to nanotechnology and microelectronics.[3,4] These compounds were also used to prepare sulfides by thermal decomposition.[3,5] Moreover, the quite different stability between lanthanide and actinide dithiocarbamates have been extensively explored to perform a selective and effective chemical separation method of 4f and 5f elements from aqueous media.[6] Although the first reports about trivalent lanthanide dithiocarbamates date back to the second half of the last century,[7–11] this class of compounds has been significantly less investigated than those containing hard donor atoms like e.g., N and O. This is probably owing to the lower affinity of hard acceptor Ln^{3+} ions to soft sulfur S-donor atoms, which may lead to less stable compounds than those containing ligands with hard donor groups. However, the ability of dithiocarbamates to act as small bite angle chelating

ligands together with the high electronic densities on the two sulfur atoms have been pointed out as the main factors that contribute to stabilize metal ion complexes in different oxidation states.[12] Currently, a large number of neutral lanthanide–dithiocarbamate complexes are known, most of them contain monodentate or bidentate auxiliary ligands. However, anionic complexes $[Ln(S_2CNR_2)_4]^-$ and neutral homoleptic complexes $Ln(S_2CNR_2)_3$ have also been prepared. Spectroscopic properties of Ln(III)-dithiocarbamates complexes (Ln= Sm, Pr, Eu, Tb and Dy) have been target of several studies.[13–16] In particular, Eu^{3+}-coordination compounds have attracted growing attention. This is due to their singular photoluminescent properties for practical applications, such as emission of pure red color that arises from intraconfigurational-$4f^6$, and as well due to both the main emitting ($^5D_0$) and the ground ($^7F_0$) states are not split by ligand field effects in chemical environments of any point symmetries.[17] Eu–dithiocarbamate complexes are usually not luminescent systems or exhibit very low luminescence intensity at room temperature, when both directly and indirectly excited. This behavior was first reported by C. K. Jørgensen, who pointed out that these complexes have (LMCT) states of very low energy,[18] which act as an efficient luminescence quenching channel. Consequently, recording the photoluminescence from Eu–dithiocarbamate compounds is generally a very difficult task. Although there is still no definitive and detailed understanding of how ligand properties lead to (LMCT) states of low energies in trivalent lanthanide compounds, many systems reported in the literature present ligands with soft donor sites. Furthermore, several studies have shown that electronic and structural features play an essential role in the electron density delocalization towards the donated site, increasing its polarizability, and consequently changing the position of the LMCT states.[19] In this vein, dithiocarbamate and their derivative compounds have been used as a well-defined platform for validating experimental and theoretical method-

[a] C. L. Teske, E. E. S. Teotonio, H. Terraschke, S. Mangelsen, W. Bensch
Institute of Inorganic Chemistry, Christian-Albrechts-Universität zu Kiel, Max-Eyth-Str. 2, D-24118 Kiel Germany
E-mail: cteske@ac.uni-kiel.de
[b] E. E. S. Teotonio
Department of Chemistry, Federal University of Paraíba, 58051-970, João Pessoa, Paraíba, Brazil

💻 Supporting information for this article is available on the WWW under https://doi.org/10.1002/zaac.202200292

ologies in investigating the intramolecular LMCT in the lanthanide complexes containing such states of low energy.[16,20] It is noteworthy that all lanthanide dithiocarbamate complexes mentioned so far contain relatively large substituent moieties (R). This inspired us to investigate the synthesis and crystal structure of two new lanthanide dithiocarbamate complexes (NH$_4$[Ln(S$_2$CNR$_2$)$_4$]·H$_2$O, Ln: La, Eu and with R=H). Herein, we also report about the spectroscopic properties of pure NH$_4$[Eu-(S$_2$CNH$_2$)$_4$]·H$_2$O and Eu^{3+}-doped NH$_4$[La$_{1-x}$Eu$_x$(S$_2$CNH$_2$)$_4$]·H$_2$O systems, where x=0.016 and 0.05, taking into account the role of the LMCT states.

Results and Discussion

Crystal structures

The crystal structures of both complexes (NH$_4$[**Eu**(S$_2$CNH$_2$)$_4$]·H$_2$O **a**) and NH$_4$[**La**(S$_2$CNH$_2$)$_4$]·H$_2$O **b**)) are isotypic (monoclinic, space group $P2_1$/c). The rare earth atoms in the complex ammonium salts are coordinated by eight next sulfur atoms (S) from four bidentate dithiocarbamate molecules. The eight Ln–S distances
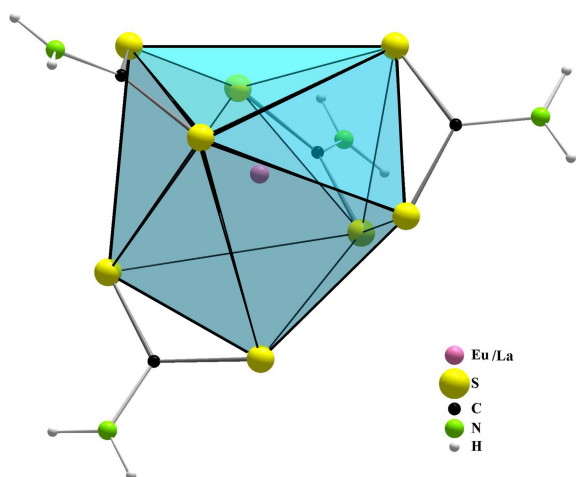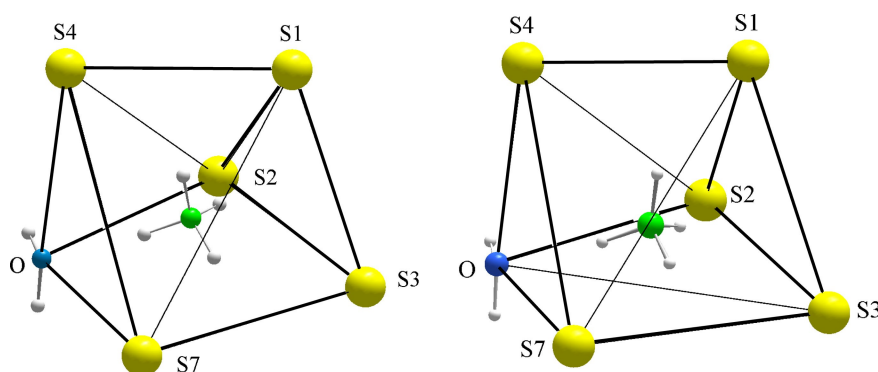
from 2.8524(10) to 2.9117(12) Å for (**a**) and 2.9441(3) to 2.9997(3) for (**b**) (Tables **S2a** and **S2b**), respectively, are very close to the sum of the ionic radii for CN=8[23] with Σ=2.916 Å for Eu^{3+}-S^{2-} and Σ=3.00 Å for La^{3+}-S^{2-}. The bite angles in the rage of 61.31 to 62.19 (**a**) and 59.90 to 60.63 (**b**), respectively (Table S2a, Table S3a), fit well with other examples from the literature [e.g., 3,22]. The shape of the coordination polyhedra around the ammonium resembles a distorted trigonal prism surrounding,[21,22] each with five sulfur atoms (S(1), S(2), (S3), S(4) and (S7)) and the O^{2-} of the H$_2$O (Figure 1, Figure 2). Actually, the interaction among the NH$_4^+$ ion and the sulfur (S) as well as the oxygen atom (O) is based on hydrogen bonds in the range of N(5)-H⋯S=2.539 to 2.874 Å for **a**) and 2.466 to 2.882 Å for **b**), respectively, and N(5)-H⋯O with 1.837 Å and 1.848 Å (see Tables **S3a** and **S3b**). Although these distances are significantly shorter than the sum of the estimated van der Waals radii (Σ= 3.0 Å[24]), the individual hydrogen bonding is at best medium strong, for the <DHA angles are significantly smaller than 180° (<DHA=119.03 to 127.87° for **a** and 115.75 to 156.98° for **b**). The N–H⋯O bonds are stronger (with <DHA=166.21 for **a** and 170.3° for **b**). Hydrogen bonding of water (O–H⋯S) is less intensive (with H⋯A in the region 2.360 to 2.467 Å and <DHA= 161.28 to 166.67°). The remaining N–H⋯S interactions of the N–H$_2$ groups are ranging from medium strong to weak (see Tables S2b, S3b). Finally, the hydrogen bonding interactions result in the linkage of the coordination polyhedra forming a 3D network (Figure 3). The steric requirements of the organic moieties (R) in the N,N–dithiocarbamates, studied so far, exert an additional structure directing effect, which does not occur here due to the small R=H. In contrast to the organo–dithiocarbamate complexes, where C–H⋯X interactions dominate, the 3D network of hydrogen bonds consists only of N–H⋯S, O–H⋯S, and N–H⋯O, which connect the [Ln(S$_2$CNH$_2$)$_4$]$^-$ building units. As a result, these building units are comparatively more densely packed (see Figure 3), compared to complexes with bulky R groups.

Figure 1. Coordination polyhedron around Eu/La in NH$_4$[**Ln**-(S$_2$CNH$_2$)$_4$]·H$_2$O.

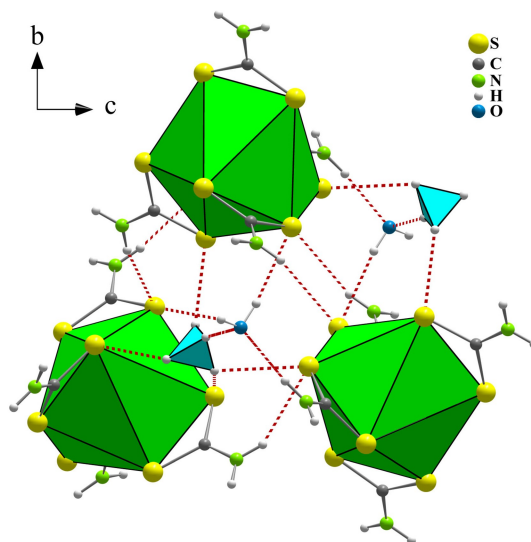**Figure 2.** Coordination polyhedra around the ammonium ions in (**a**) (left) and in (**b**) right.

Figure 3. Three-dimensional arrangement of the polyhedra in $NH_4[Ln(S_2CNH_2)_4] \cdot H_2O$ (Viewing direction along [100]). Hydrogen bonds are shown as dashed red lines.

Optical Properties

Figure 4 depicts crystals of the $NH_4[Eu(S_2CNH_2)_4] \cdot H_2O$ (Figure 4a) and $NH_4[La(S_2CNH_2)_4] \cdot H_2O$ (Figure 4b) complexes, which are orange and colorless, respectively. It has also been observed that even Eu-doped $NH_4[La_{1-x}Eu_x(S_2CNH_2)_4] \cdot H_2O$ (x = 0.016 and 0.05) systems show slightly yellowish colors. This feature may suggest the presence of a dithiocarbamate–Eu^{3+} charge transfer state of low energy in the compounds containing the Eu^{3+} ion. It is worthy of mention that the pure and Eu-doped $NH_4[La_{1-x}Eu_x(S_2CNH_2)_4] \cdot H_2O$ (x = 0.016 and 0.05) complexes do not exhibit luminescence to the naked eye under UV-VIS light, indicating that the LMCT state is also acting as an efficient luminescence quenching channel for the Eu^{3+} ion. However, stronger evidence for the presence of a LMCT state can be obtained from the spectroscopic data. Figs. S3 and S4 (see **ESI**) show the diffuse reflectance spectra for the $NH_4[Eu(S_2CNH_2)_4] \cdot H_2O$ and $NH_4[La(S_2CNH_2)_4] \cdot H_2O$. The sigmoid-Boltzmann function was applied to the reflectance bands and display that both investigated complexes present an optical band gap

of 3.5 eV. Furthermore, a comparison between the diffuse reflectance spectra in the range from 2.3 to 3.2 eV reveals the presence of a low-intensity broad band that appears only in the Eu^{3+} ion complex. This band may be assigned to a transition from the singlet ground state (S_0) to dithiocarbamate-Eu^{3+} charge transfer state ($S_0 \rightarrow LMCT$).

Infrared spectrum

From the MIR measurement[25] (Figure 5), the characteristic bands of the dithiocarbamate ligand are visible. The N–H valence and deformation vibrations are at 3320, 3242, 3146 and 1595 cm^{-1}. The band at 1376 cm^{-1} is in the region of the C–N valence vibration, and the band at 1180 cm^{-1} is in that of the C=S. Moreover, the valence vibration of the N–C–S bond occurs at 845 cm^{-1}.[26]
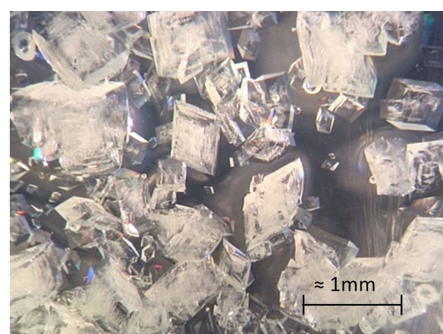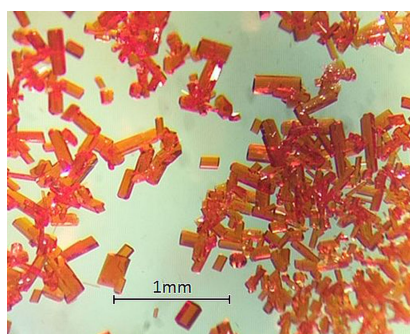

Figure 4. Picture of the crystals of the $NH_4[Eu(S_2CNH_2)_4] \cdot H_2O$ (left) and (b) $NH_4[La(S_2CNH_2)_4] \cdot H_2O$ (right) complexes.
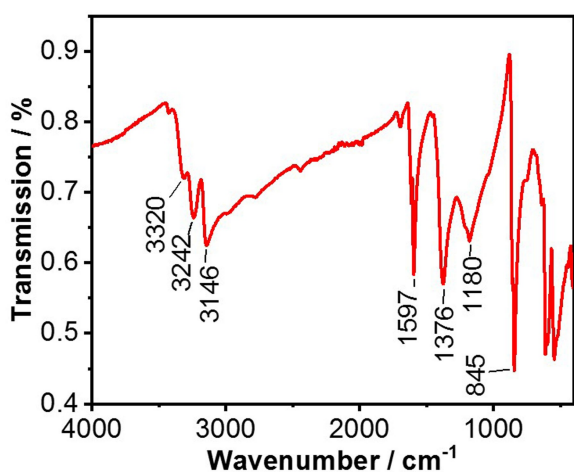
Figure 5. MIR spectrum of $NH_4[Eu(S_2CNH_2)_4] \cdot H_2O$. The characteristic bands are labeled.

Photoluminescent studies

Excitation spectra of the $NH_4[Eu(S_2CNH_2)_4] \cdot H_2O$ and Eu-doped $NH_4[La_{1-x}Eu_x(S_2CNH_2)_4] \cdot H_2O$ (x = 0.016 and 0.05) compounds recorded at room temperature (~298 K) under emission at 613 nm ($^5D_0 \rightarrow ^7F_2$ of the Eu^{3+} ion) are shown in Figure 6a–6c. Overall, these spectra show narrow weak peaks from the intraconfigurational-4f transitions centered on the Eu^{3+} ion:

$^7F_0 \rightarrow ^5D_4$ (362 nm), $^7F_0 \rightarrow ^5G_{6,4,2}$ (383 nm), $^7F_0 \rightarrow ^5L_6$ (393 nm), $^7F_0 \rightarrow ^5D_2$ (463 nm), $^7F_0 \rightarrow ^5D_1$ (525 nm) and $^7F_1 \rightarrow ^5D_1$ (534 nm).[27] It is also important to notice a presence of a broad band for the Eu-doped $NH_4[La_{1-x}Eu_x(S_2CNH_2)_4] \cdot H_2O$ (x = 0.016 and 0.05) solid solutions in the spectral range from 400 to 570 nm, which can be assigned to the LMCT transition. The absence of this band in the excitation spectra of the $NH_4[Eu(S_2CNH_2)_4] \cdot H_2O$ complex may be due to the strong self-quenching effect, caused by the overlap between the emission and absorption bands. This finding suggests that the luminescence quenching effect of the charge transfer state may be dependent on the Eu^{3+} ion concentration in the mixed crystals.

Figures 7a–7b show the emission spectra for $NH_4[Eu(S_2CNH_2)_4] \cdot H_2O$ and Eu-doped solid solutions $NH_4[La_{1-x}Eu_x(S_2CNH_2)_4] \cdot H_2O$ (x = 0.016 and 0.05), recorded at room temperature (~298 K) under excitation at 393 nm ($^7F_0 \rightarrow ^5L_6$ of the Eu^{3+} ion). In general, these spectra are characterized by a broad emission band, covering the entire spectral range that is probable from LMCT transition. In addition, it also shows narrow emission bands assigned to the $^5D_0 \rightarrow ^7F_J$ (J = 1, 2, 3, and 4) transitions. Interestingly, the band due to the $^5D_0 \rightarrow ^7F_4$ transition at 720 nm exhibits significant high relative intensity. This result is in agreement with the crystallographic data for slightly distorted dodecahedron coordination polyhedra with symmetries belonging to the D_{2d} point group. The decrease in the relative intensity of this band for the Eu-doped $NH_4[La_{1-x}Eu_x(S_2CNH_2)_4] \cdot H_2O$ systems, as compared with the pure Eu–dithiocarbamate, reflects greater structural distortions due

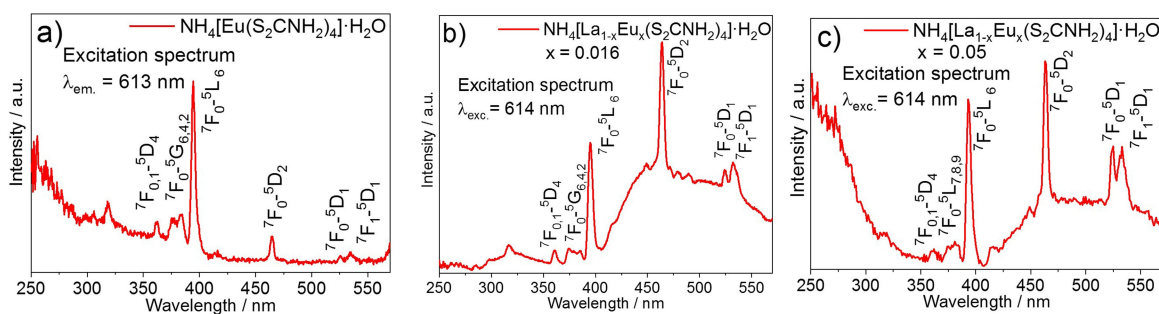**Figure 6.** Excitation spectra of Eu^{3+}-dithiocarbamate complexes: a) $NH_4[Eu(S_2CNH_2)_4] \cdot H_2O$ and Eu-doped $NH_4[La_{1-x}Eu_x(S_2CNH_2)_4] \cdot H_2O$, b) x = 0.016 and c) x = 0.05), recorded at room temperature under emission monitored at 613 nm on the $^5D_0 \rightarrow ^7F_2$ transition of the Eu^{3+} ion.
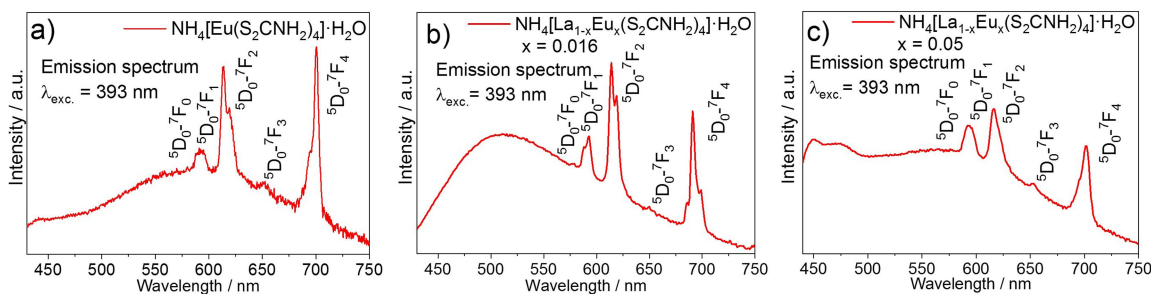
Figure 7. Emission spectra of Eu^{3+}-dithiocarbamate: a) $NH_4[Eu(S_2CNH_2)_4] \cdot H_2O$ and Eu-doped $NH_4[La_{1-x}Eu_x(S_2CNH_2)_4] \cdot H_2O$, b) x = 0.016 and c) x = 0.05), recorded at room temperature under excitation monitored at 393 nm on the $^7F_0 \rightarrow ^5L_6$ transition of the Eu^{3+} ion.

to the difference between the ionic radii of the La^{3+} and Eu^{3+} ions.

Conclusion

The above investigation has shown that the Ln(III) dithiocarbamates $NH_4[Eu(S_2CNH_2)_4] \cdot H_2O$ (**a**) and $NH_4[La(S_2CNH_2)_4] \cdot H_2O$ (**b**) can be crystallized from *concentrated* aqueous solutions of the reactants $Ln(NO_3)_3 \cdot 6H_2O$ and $NH_4S_2CNH_2$, as described (vide supra). Based on single crystal X-ray diffraction studies, the coordination sphere of the Ln^{3+} cations can be classified into the already known structural patterns of other rare earth dithiocarbamates [e.g.,13,15]. The crystal structures of (**a**) and (**b**) are isotypic, which provides a promising possibility for incorporation of Eu^{3+} into the lattice of the La-compound, an attractive field of exploration for optical investigations. Indeed, the solid solutions $NH_4[La_{1-x}Eu_x(S_2CNH_2)_4] \cdot H_2O$ (x=0.016 and x=0.05) could be synthesized. Based on the spectral data, we propose an energy diagram illustrating a channel for depopulation of the excited levels of the Eu^{3+} ion in the dithiocarbamate complex via LMCT state (Figure 8). According to this proposal, the following mechanisms are operative in this system: a) Excitation of a dithiocarbamate molecule ($S_0 \rightarrow S_1$); b) intersystem crossing (ISC) from the singlet to the low-lying excited triplet state ($S_1 \rightarrow T_1$); c) intramolecular energy transfer (IET) from the T_1 state to LMCT or to the Eu^{3+} excited levels. Furthermore, even by direct excitation on the excited states of the Eu^{3+} ion, the LMCT state promotes a very efficient energy back transfer effect, which drastically reduces the population of the excited states of the metal center. As a result, the emission intensity of the lanthanide ion is almost completely quenched. This spectroscopic behavior is in line with the results predicted by Faustino and collaborators through a theoretical approach,[28] for coordination compounds with LMCT energy in the 5000–20000 cm^{-1} interval.
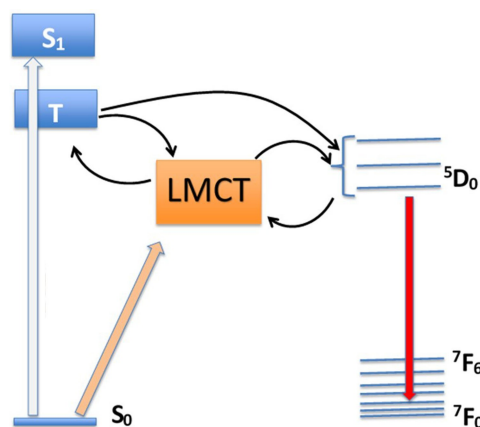

Figure 8. Qualitative energy level diagram highlighting the main energy transfer mechanism in the $NH_4[Eu(S_2CNH_2)_4] \cdot H_2O$ complex. The full and narrow arrows represent radiative (absorption or emission) and non-radiative energy transfer, respectively.

Experimental Section

Preparation

The title compounds were prepared by co-precipitation from aqueous solutions.

a) $NH_4[Eu(S_2CNH_2)_4] \cdot H_2O$: $Eu(NO_3)_3 \cdot 6H_2O$ (1.338 g; 3 mmol) was dissolved in ca. 3 mL H_2O on a flat watch glass (Ø 20 cm) and freshly prepared, colorless $NH_4S_2CNH_2$[29] (1.488 g; 13.5 mmol) was added. Then, after with stirring all $NH_4S_2CNH_2$ had dissolved, the water was evaporated at RT until a red crystal paste had formed (Figure 4a). For this purpose, the watch glass was positioned in the fume hood in such a way that it was overflowed by a constant stream of air. The residual liquid with the precipitated crystals was sucked off through a *Hirsch funnel*, washed with approx. 1 mL each of ethanol (total approx. 6 mL), dried in vacuo, and finally stored in the freezer.

b) $NH_4[La(S_2CNH_2)_4] \cdot H_2O$: The preparation was similar to that described under **a**. First of all, the solubility of the lanthanum dithiocarbamate (**b**) in H_2O was found to be considerably better than that of the homologue Eu-compound. The watch glass, containing the solution of 1.763 g $La(NO_3)_3 \cdot 6H_2O$ (4 mmol) + 1.8 g colorless $NH_4S_2CNH_2$ (16.3 mmol) in ca. 4 mL H_2O, was positioned in the fume hood as described in section a), but on a sand bath with *temperature control*. Evaporation was carried out at 50–55 °C. After ca. three hours, a syrupy slurry had formed containing colorless transparent coarse crystals (Figure 4b). It was sucked off through a *Hirsch funnel* and treated as mentioned above. Both dithiocarbamates ($NH_4[Eu(S_2CNH_2)_4] \cdot H_2O$ and $NH_4[La(S_2CNH_2)_4] \cdot H_2O$) are stable only for several days at room temperature, but can be stored for a longer time closed in the freezer without further precaution.

Preparation of solid solutions

The solid solutions $NH_4[La_{x-1}Eu_x(S_2CNH_2)_4] \cdot H_2O$ (x=0.016 and x=0.05) were synthesized by triturating the mixtures of Ln-compounds with the desired molar ratio in an agate mortar, using various fluids. About 0.1 g each of the mixture of $NH_4[La(S_2CNH_2)_4] \cdot H_2O$ plus $NH_4[Eu(S_2CNH_2)_4] \cdot H_2O$, in the desired molar ratio (ca. 0.95/0.05 and 0.98/0.02), was triturated together with ca. $^1/_2$ mL petroleum gasoline (40–60°). After drying, the procedure was repeated (approx. 3–4 times) until no more red crystals were visible under the light microscope. The solvent, used for solid solution formation, consisted of 10 mL MeOH + 0.5 mL H_2O. Of this, two drops were added at a time during triturating. This was repeated 2–3 times after drying. Finally, a pale yellow, microcrystalline powder was obtained.

We note: The values given for x *were calculated from the weighted sample*. Therefore, they do *not* have to agree *exactly* with the real composition.

Elemental Analysis

The percent composition data (C, N, H, S; standard deviation in brackets) were determined by combustion analysis on a CHNS-Rapid-Element-Analyzer (Heraeus GmbH) using sulfanilamide as standard. $NH_4[Eu(S_2CNH_2)_4] \cdot H_2O$ (556.68 g·mol^{-1}): C 8.55(2) (calcd. 8.63); H 2.56(5) (calcd. 2.55); N 12.74(6) (calcd. 12.58); S 44.7(3) (calcd. 46.08); $NH_4[La(S_2CNH_2)_4] \cdot H_2O$ (543,62 g·mol^{-1}): C 8.59(4) (calcd. 8.84); H 2.69(7) (calcd. 2.60); N 12.51(6) (calcd. 12.88); S 48.4(1) (calcd. 47.2) %.

Single-crystal X-ray Investigation

a) $NH_4[Eu(S_2CNH_2)_4] \cdot H_2O$

The single-crystal X-ray diffraction data were collected on a STOE Imaging Plate Diffraction System (IPDS-2) with graphite mono-chromatized Mo-K_α radiation ($\lambda = 0.7107$ Å) at 200(2) K. After the correction of the raw data for Lorentz and polarization effects, the absorption correction was applied using X-RED[30] and X-Shape.[31] The SHELXL-2014 program package[32] was used to solve the crystal structure by Direct Methods.

b) $NH_4[La(S_2CNH_2)_4] \cdot H_2O$

The single-crystal X-ray diffraction was collected with an XtaLAB Synergy-S diffraction system equipped with micro-focus source (PhotonJet-S) and a HyPix-6000HE Hybrid Photon Counting (HPC) detector using monochromatized Mo-K_α radiation ($\lambda = 0.7107$ Å) at 100(2) K. The absorption correction was applied using *CrysAlisPro* 1.171.42.58a; Rigaku Oxford Diffraction, 2022.[33] For the structure solution SHELXT[34] was applied. Both compounds crystallize in the monoclinic space group $P2_1/c$ (No. 14). The SHELXL-2014 program

package[32] was used to solve the crystal structure, and the refinement was performed against F^2. The non-hydrogen atoms were refined with anisotropic displacement parameters. The hydrogen atoms of the amino groups were allowed to ride on their parent atoms with idealized geometry and were refined with fixed bond lengths (N–H = 0.88 Å) for **a**) and with isotropic displacement parameters for **b**). Fixed isotropic displacement parameters [$U_{iso}(H) = 1.2\ U_{eq}(N)$] were used. An ideal tetrahedral H–N–H angle was assumed for the ammonium ions, where the corresponding H–H distances are 1.486 Å.[35] The atomic positions of hydrogen were refined applying these values in the SHELXL-97 restraints[32] (DFIX 0.91 0.02N(5), H(i) (i = 6 to 9) for the N–H bond lengths). Fixed isotropic displacement parameters [$U_{iso}(H) = 1.5\ U_{eq}(N)$] were used. After locating water hydrogen atoms using the difference electron density map, their positions were refined with O–H distances restrained to 0.840(01), [$U_{iso}(H) = 1.5\ U_{eq}(O)$]. More technical details of the data acquisition and selected refinement results are summarized in Table 1. The final atomic coordinates as well as the equivalent isotropic displacement parameters are listed in Table S1. Table S2a, Table S2b, Table S3a and Table S3b (see **ESI**) show the lists of the shortest interatomic distances, selected bond angles, and geometric parameters of possible hydrogen-bonding interac-

Table 1. Crystal data and structure refinement for $NH_4[Eu(S_2CNH_2)_4] \cdot H_2O$ (**a**) and $NH_4[La(S_2CNH_2)_4] \cdot H_2O$ (**b**).

	(a)	(b)
Empirical formula	$C_4 H_{14} Eu N_5 O S_8$	$C_4 H_{14} La N_5 O S_8$
Formula weight	556.64	543.59
Temperature/K	200(2)	100(2)
Diffractometer	STOE IPDS-2	XtaLAB Synergy, Dualflex, HyPix
Wavelength/Å	0.71073	0.71073
Crystal system	monoclinic	monoclinic
Space group	$P2_1/c$	$P2_1/c$
a/Å	8.4461(3)	8.5048(1)
b/Å	13.6367(3)	13.8448(2)
c/Å	16.2945(5)	16.2082(2)
α/°	90	90
β/°	103.759(2)	103.764(2)
γ/°	90	90
Volume/Å^3	1822.90(10)	1853.66(4)
Z	4	4
Density (calculated) Mg/m^3	2.021	1.948
Absorption coefficient/mm^{-1}	4.354	3.203
F(000)	1088	1064
Crystal size/mm^3	0.153×0.107×0.068	0.148×0.106×0.072
θ range for data collection/°	1.971 to 27.313	2.466 to 33.485
Index ranges	−10 < = h < =10	−12 < = h < =13
	−17 < = k < =17	−20 < = k < =21
	−21 < = l < =21	−24 < = l < =24
Reflections collected	20856	65326
Independent reflections	4087	6781
$R_{(int)}$	0.0670	0.0140
Completeness/%	99.7	100.0
Absorption correction	numerical	multi-scan
Max. and min. transmission	0.6265/0.4098	1.0/0.91614
Refinement method	Full-matrix least-squares on F^2	
Data/restraints/parameters	4087/13/196	6781/13/190
Goof (F^2)	1.129	1.040
R_1 [I > 2sigma(I)]	0.0358	0.0153
wR_2	0.0900	0.0363
R indices (all data)	0.0422	0.0164
wR_2	0.0933	0.0367
Extinction coefficient	0.0048(5)	n/a
$\triangle\rho$/e·Å^{-3} (max./min.)	0.185/−0.100	2.019/−0.957

tions. Graphical representations of the structure were produced with the program Diamond.[36]

Crystallographic data (including structure factors) for the structures in this paper have been deposited at the Cambridge Crystallographic Data Centre, CCDC, 12 Union Road, Cambridge CB21EZ, UK. Copies of the data can be obtained free of charge on quoting the depository number CCDC-2203537 for $NH_4[\textbf{Eu}(S_2CNH_2)_4]\cdot H_2O$ and CCDC-2203538 for $NH_4[\textbf{La}(S_2CNH_2)_4]\cdot H_2O$ (Fax: +44-1223-336-033; E-Mail: deposit@ccdc.cam.ac.uk; http://www.ccdc.cam.ac.uk).

X-ray Powder Diffraction

XRPD patterns were collected on a Panalytical Empyrean diffractometer equipped with a PIXcel 1D detector using nickel filtered Cu-K$_\alpha$ radiation. The samples were measured in transmission geometry as flat plates at room temperature. The structure data from single crystal X-ray diffraction were used to calculate the theoretical powder patterns (comparison of the experimental and calculated XRPD (see **ESI**, Figs. S4, S5).

UV/VIS spectroscopy

For the collection of the reflectance spectra an UV/VIS-NIR-two-channel spectrometer Cary 5000 Instrument Version 1.12 (Varian Techtron Pty., Darmstadt) was employed. The spectra were transformed into absorption spectra through the Kubelka-Munk function $\alpha/S=(1-R)^2/2R$, ($\alpha=$absorption coefficient, $R=$reflectance with given wave length and $S=$scattering coefficient).[37] The optical band gap was estimated from the intersection point between the abscissa and the tangent to the linear part of the absorption edge in the plot $\alpha/S=f(Eg)$ (**see ESI**, Figure S6 and Figure S7). $BaSO_4$ powder was used as white standard.

MIR spectroscopy

A Bruker Alpha-p, ATR spectrometer (4000 cm^{-1}–450 cm^{-1}) was used to record the MIR spectrum.

Luminescence measurements

Luminescence measurements were carried out with a FL322 Fluorolog-3 fluorescence spectrometer (HORIBA Jobin Yvon GmbH), containing a 450 W xenon lamp, a R928P photomultiplier, iHR-320-FA triple grating imaging spectrograph, and a Syncerity CCD detector. The solid samples were measured at room temperature in Suprasil® quartz ampoule.

Acknowledgements

Conflict of Interest

The authors declare no conflict of interest.

Data Availability Statement

The data that support the findings of this study are openly available in Cambridge Crystallographic Data Centre at http://www.ccdc.cam.ac.uk, reference number 2203537.

[1] J. A. Vale, W. M. Faustino, P. H. Menezes, G. F. de Sá, *J. Braz. Chem. Soc.* **2006**, *17*, 829–831.

[2] Ponnuchamy Pitchaimani, K. M. Lo, K. P. Elango, *Polyhedron* **2013**, *54*, 60–66.

[3] M. D. Regulacio, N. Tomoson, S. L. Stoll, *Chem. Mater.* **2005**, *17*, 3114–3121.

[4] N. Pradhan, S. J. Efrima, *Am. Chem.* **2003**, *125*, 2050–2051.

[5] W. L. Boncher, M. D. Regulacio, S. L. Stoll, *J. Solid State Chem.* **2010**, *183*, 52–56.

[6] N. P. Bessen, J. A. Jackson, M. P. Jensen, J. C. Shafer, *Coord. Chem. Rev.* **2020**, *421*, 213446.

[7] D. Brown, D. G. Hola, *Chem. Comm.* **1968**, *23*, 1545–1546.

[8] M. Ciampolini, N. Nardi, P. Colamarino, P. Orioli, *J. Chem. Soc., Dalton Trans.* **1977**, *4*, 379–384.

[9] Tang Ning, Gan Xinmin, Zhu Hhailiang, Tan Minyu, *Polyhedron* **1990**, *9*, 859–862.

[10] Z. Hailiang, T. Ning, G. Ximin, Z. Weiguang, T. Minyu, W. Aili, *Polyhedron* **1993**, *12*, 945–948.

[11] Lu Wenjie, Wang Xingtang, Han Xiajun, Chen Min, *Polyhedron* **1992**, *11*, 1815–1819.

[12] A. T. Odularu, P. A. Ajibade, *Bioinorg. Chem. Appl.* **2019**, *8260496*, 1–15.

[13] P. Pitchaimani, K. M. Lo, K. P. Elango, *Polyhedron* **2015**, *93*, 8–16.

[14] A. Zubair, K. Iftikhar, *Inorg. Chim. Acta* **2012**, *392*, 165–176.

[15] M. D. Regulacio, M. H. Pablico, J. A. Vasquez, P. N. Myers, S. Gentry, M. Prushan, S.-W. Tam-Chang, S. L. Stoll, *Inorg. Chem.* **2008**, *47*, 1512–1523.

[16] W. M. Faustino, O. L. Malta, E. E. S. Teotonio, H. F. Brito, A. M. Simas, G. F. de Sá, *J. Phys. Chem. A* **2006**, *110*, 2510–2516.

[17] A. N. Carneiro Neto, E. E. S. Teotonio, G. F. de Sá, H. F. Brito, J. Legendziewicz, L. D. Carlos, M. C. F. C. Felinto, P. Gawryszewska, R. T. Moura Jr., R. L. Longo, W. M. Faustino, O. L. Malta, in *Handbook on the Physics and Chemistry of Rare Earths*, volume 56, Elsevier, **2019**, 55–162.

[18] C. K. Jørgensen *Mol. Phys.* **1962**, *5*, 271–277.

[19] K. P. Zhuravlev, V. I. Tsaryuk, A. V. Vologzhanina, P. P. Gawryszewska, V. A. Kudryashova, Z. S. Klemenkova, *ChemistrySelect* **2016**, *1*, 3428–3437.

[20] G. K. Liu, M. P. Jensen, P. M. Almond, *J. Phys. Chem. A* **2006**, *110*, 2082–2088.

[21] J. L. Hoard, J. V. Silverton, *Inorg. Chem.* **1963**, *2*, 235–242.

[22] C. Su, M. Tan, N. Tang, X. Gan, Z. Zhang, Q. Xue, K. Yu, *Polyhedron* **1997**, *16*, 1643–1650.

[23] R. D. Shannon, *Acta Crystallogr. Sect. A* **1976**, *32*, 751–767.

[24] A. Bondi, *J. Phys. Chem.* **1964**, *68*, 441–451.

[25] A. Harder, *Bachelor Thesis*, Univ. Kiel **2020**.

[26] C. N. R. Rao, R. Venkataraghavan, *Spectrochim. Acta* **1962**, *18*, 541–547.

[27] Y. C. Miranda, L. L. A. L. Pereira, J. H. P. Barbosa, H. F. Brito, M. C. F. C. Felinto, O. L. Malta, W. M. Faustino, E. E. S. Teotonio, *Eur. J. Inorg. Chem.* **2015**, *27*, 3019–3027.

[28] W. M. Faustino, O. L. Malta, G. F. de Sa, *J. Chem. Phys.* **2005**, *122*, 054109.

[29] C. L. Teske, W. Bensch, *Z. Anorg. Allg. Chem.* **2010**, *636*, 356–362.

[30] X-RED, Data Reduction Program, Version 1.11, Stoe & Cie GmbH, **1998**.

[31] X-SHAPE, Version 1.03, Stoe & Cie GmbH, Darmstadt, Germany, **1998**.

[32] SHELXL-2014-Crystal Structure Refinement-Multi-CPU Version 2014/7, G. M. Sheldrick, *Acta Crystallogr. Sect. A* **2008**, *64*, 112–122.

[33] CrysAlis Pro, *https://rigaku.com/products/crystallography/chrysalis*.

[34] SHELXT, G. M. Sheldrick, *Acta Crystallogr. Sect. A* **2015**, *71*, 3–8.

[35] J. Fábry, R. Krupková, I. Císařová, *Acta Crystallogr. Sect. E* **2003**, *59*, i14–i16.

[36] Diamond – Crystal and Molecular Structure Visualization Crystal Impact – K. Brandenburg & H. Putz GbR, Rathausgasse 30, D-53111 Bonn.

[37] P. Kubelka, F. Munk, *Z. Tech. Phys.* **1931**, *12*, 593–601.